

## New measurement of the $\Lambda$ helicity in the decay $\Xi^0 \rightarrow \Lambda \pi^0$

G. Bunce,\* R. Handler, R. March, P. Martin,<sup>†</sup> L. Pondrom, and M. Sheaff  
*Department of Physics, University of Wisconsin, Madison, Wisconsin 53706*

K. Heller, O. E. Overseth, and P. Skubic<sup>‡</sup>  
*Department of Physics, University of Michigan, Ann Arbor, Michigan 48109*

T. Devlin, B. Edelman,<sup>§</sup> R. T. Edwards,<sup>¶</sup> L. Schachinger, and S. P. Yamin\*  
*Department of Physics, Rutgers, The State University, Piscataway, New Jersey 08854*

(Received 27 February 1978)

A sample of 6075 decays of unpolarized  $\Xi^0$  hyperons has been obtained in the Fermilab neutral-hyperon beam. All decay products from the sequence  $\Xi^0 \rightarrow \pi^0 \Lambda$ ,  $\pi^0 \rightarrow \gamma \gamma$ ,  $\Lambda \rightarrow p \pi^-$  were detected. Analysis of the proton asymmetry in the  $\Lambda$  decay gave  $\alpha_{\pm^0} \alpha_{\Lambda} = -0.317 \pm 0.027$  or  $\alpha_{\pm^0} = -0.490 \pm 0.042$ . A comparison with the world average for  $\alpha_{\pm^-}$  gives a  $\Delta I = 3/2$  amplitude of  $25 \pm 9\%$ .

### INTRODUCTION

The weak nonleptonic decays of the hyperons may be described in terms of isospin-changing  $s$ -wave and  $p$ -wave amplitudes. Clebsch-Gordan coefficients of the isospin-changing amplitudes link the experimental observables for decays within the same isospin family. It has been observed that  $\Delta I = \frac{1}{2}$  terms dominate these hyperon decays, although the theoretical basis for this is not well understood.

Experimentally, these amplitudes are determined by comparing the decay probabilities and asymmetry parameters of the members of a given isotopic-spin multiplet within the hyperon family. We use the symbol convention  $s_{2\Delta I}$  and  $p_{2\Delta I}$  to refer to  $s$ - and  $p$ -wave transitions with isotopic-spin change  $\Delta I$ .

For  $\Lambda$  decay, experiment indicates a small  $\Delta I = \frac{3}{2}$   $s$ -wave amplitude:  $s_3/s_1 = 0.027 \pm 0.008$ .<sup>1</sup> This arises almost entirely from the ratio of decay rates for  $\Lambda \rightarrow p \pi^-$  and  $\Lambda \rightarrow n \pi^0$ . The ratio of the asymmetry parameters is less accurately measured, but is consistent with the  $\Delta I = \frac{1}{2}$  rule, yielding a  $p$ -wave  $\Delta I = \frac{3}{2}$  amplitude:  $p_3/p_1 = 0.030 \pm 0.037$ .<sup>1</sup> The ultimate precision of the test of the  $\Delta I = \frac{1}{2}$  rule in a  $\Lambda$  decay appears to be limited by the experimental difficulty in detecting the neutral-decay mode  $\Lambda \rightarrow n \pi^0$  as well as by uncertainties in the calculation of the radiative corrections.<sup>2</sup>

The analysis of  $\Sigma$  decay is more complex since three decays are involved. Moreover, owing to the possibility of  $\Delta I = \frac{5}{2}$  amplitudes present in this case, the interpretation is likely to remain ambiguous.<sup>3</sup>

On the other hand,  $\Xi$  decay is particularly well suited for testing the  $\Delta I = \frac{1}{2}$  rule. There are no  $\Delta I = \frac{5}{2}$  amplitudes possible as in  $\Sigma$  decay. In con-

trast to  $\Lambda$  decay,  $\Xi$  analysis does not require knowledge of final-state-interaction phase shifts because the isospin of the final state for both charged and neutral  $\Xi$  decays is the same. Furthermore, radiative corrections are smaller due to fewer charged particles in the final state.<sup>4</sup> Thus the comparison of decay rates and asymmetries of  $\Xi^-$  and  $\Xi^0$  appears to offer promise for useful tests of the  $\Delta I = \frac{1}{2}$  rule. Past experiments have had limited sensitivity due to the small number of  $\Xi^0 \rightarrow \Lambda \pi^0$  decays observed. However, since the limit on the  $\Delta I = \frac{3}{2}$   $p$ -wave amplitude in  $\Xi$  decay allows a large contribution,  $p_3/p_1 = -0.13 \pm 0.15$ ,<sup>1</sup> it is of interest to improve the measurement of the asymmetry parameter for  $\Xi^0$  decay. The advent of high-energy beams of short-lived neutral particles now allows this decay to be studied in large numbers.

This paper reports a measurement of the  $\Xi^0$  asymmetry parameter  $\alpha_{\pm^0}$  based on an analysis of 6075 decays, representing a more than threefold increase over the previous world sample. The daughter  $\Lambda$  from the principal decay mode of the  $\Xi^0$  hyperon,  $\Xi^0 \rightarrow \pi^0 \Lambda$ , is longitudinally polarized in the  $\Xi^0$  rest frame. This polarization  $\alpha_{\pm^0}$  is measured using the self-analyzing property of the  $\Lambda \rightarrow p \pi^-$  decay. Combined with the measured asymmetry parameter for the experimentally more accessible decay  $\Xi^- \rightarrow \pi^- \Lambda$ , the data allow the  $\Delta I = \frac{3}{2}$  contribution to be isolated. The following sections discuss the apparatus and data collection, the selection of  $\Xi^0$  candidates, and the measurement of  $\alpha_{\pm^0}$ .

### APPARATUS

$\Xi^0$  hyperons were produced in a 15-cm-long 6-mm-diameter beryllium target by a 400-GeV/ $c$

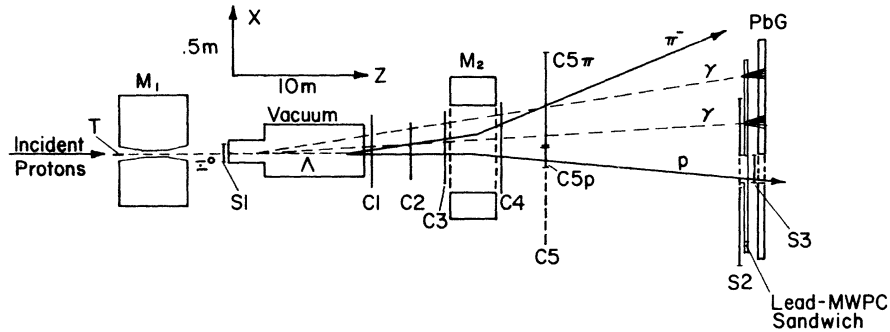


FIG. 1. A typical  $\Xi^0 \rightarrow \Lambda \pi^0$ ,  $\Lambda \rightarrow p \pi^-$ ,  $\pi^0 \rightarrow \gamma \gamma$  event is superimposed on the top view of the apparatus. S1–S3 are scintillation counters; V is the decay volume; C1–C5 are MWPC's; M2 is the analyzing magnet; PbG is the lead-glass array. C5p and C5 $\pi$  represent two sections of C5 used in the  $\Xi^0$  trigger. The trigger consisted of  $T("Xi^0") = C1 \cdot C2 \cdot C3 \cdot C4 \cdot C5p \cdot C5\pi \cdot S3 \cdot G \cdot \overline{S1} \cdot \overline{S2}$ , where G represents a sum of lead-glass signals (see text).

incident proton beam at Fermilab in the neutral-hyperon beam. A 5.3-meter-long magnetic channel cleared charged particles from the beam and defined a  $1.2\text{-}\mu\text{sr}$  solid angle for neutral-particle production (Fig. 1). The production angle was  $0^\circ$ , where transverse  $\Xi^0$  polarization is forbidden by rotational invariance and longitudinal polarization is forbidden by parity conservation in strong interactions. Our measurements confirm that the  $\Xi^0$  sample used here was unpolarized to  $\pm 4\%$  and we assumed that the polarization was exactly zero.

All products of the decay sequence  $\Xi^0 \rightarrow \pi^0 \Lambda$ ,  $\pi^0 \rightarrow \gamma \gamma$ ,  $\Lambda \rightarrow p \pi^-$  were observed in a spectrometer and lead-glass calorimeter. A decay volume 12 meters long was followed by the spectrometer consisting of six multiwire proportional chambers (MWPC's), and an analyzing magnet which gave a  $0.95\text{-GeV}/c$  transverse momentum, deflecting protons toward  $-\hat{x}$  in Fig. 1. The lead-glass array consisted of 71  $10\text{-cm} \times 10\text{-cm} \times 38\text{-cm}$  lead-glass blocks stacked in five rows with their long axes parallel to the beam direction. It was placed behind the spectrometer to detect the  $\gamma$ 's from  $\pi^0$  decay. To improve spatial resolution of a subsample of  $\gamma$ 's, a 2-radiation-length lead sheet and an MWPC were placed just upstream of the lead-glass array.

A  $\Xi^0$  trigger was used which employed various features of the decay chain  $\Xi^0 \rightarrow \Lambda \pi^0$ ,  $\Lambda \rightarrow p \pi^0$ ,  $\pi^0 \rightarrow \gamma \gamma$ . The proton and  $\pi^-$  from  $\Lambda$  decay each illuminated fairly well-defined areas of the detectors downstream of the spectrometer magnet. This fact was used to produce the highly selective electronic trigger described in Fig. 1. The first part of the trigger required at least one hit in each of the first four MWPC's (C1, C2, C3, C4) with scintillator S1 in anticoincidence. Downstream of the spectrometer magnet, the proton remained to the right ( $-x$ ) and near the beam centerline, passing through a 12.8-cm-wide area (C5p) of C5 and a

20-cm  $\times$  10-cm scintillation counter S3 in front of the calorimeter. This logic selected positive particles with momenta  $70\text{--}340\text{ GeV}/c$  and thus provided a  $\Lambda$  signature because the proton from  $\Lambda$  decay carries most of the  $\Lambda$  momentum in the laboratory. The  $\pi^-$  passed through the left ( $+x$ ) side (C5 $\pi$ ) of C5 and usually missed the detectors in the calorimeter area.

It was difficult to analyze events in which charged particles struck the calorimeter, adding energy unrelated to  $\gamma$  showers. For this reason, the two lead-glass cells in a 20-cm  $\times$  10-cm area behind S3 were removed to allow the proton to pass through. In addition, another scintillator S2 covered the front of the calorimeter except for a hole in front of the empty cells and S3, and four blocks on the  $\pi^-$  side of the array. It was used in anticoincidence to veto the few events in which any stray charged particle struck the trigger region of the glass. Most of the protons and  $\pi^-$  missed S2. An acceptable reconstructed  $\Lambda$  was obtained from 76% of these triggers.

In order to enhance the fraction  $\Xi^0$  hyperons in the trigger, the pulses from the lead-glass counters shielded by the veto S2 were summed and put into a discriminator G. (The cell in the neutral beam was left out of the trigger because of a high accidentals rate.) The threshold pulse height was set to correspond to 2 GeV of energy deposited in the calorimeter. The output of this discriminator was put into coincidence with the  $\Lambda$  signal to form the " $\Xi^0$ " trigger. This requirement was fulfilled for 8% of the  $\Lambda$  signals. The full trigger requirement from the detector elements was the coincidence

$$T("Xi^0") = C1 \cdot C2 \cdot C3 \cdot C4 \cdot C5p \cdot C5\pi \cdot S3 \cdot G \cdot \overline{S1} \cdot \overline{S2}.$$

The lead-glass array was calibrated with electrons and positrons from  $\gamma$  conversions in the neu-

tral beam. These were obtained in special runs with a lead converter and a small magnet (bending vertically) upstream of S1. The  $e^+e^-$  pairs were first split vertically by the upstream magnet, and then horizontally by the spectrometer. The event trigger was modified to accept such events. All MWPC coordinates on the  $e^+$  and  $e^-$  trajectories through the spectrometer and the lead-glass pulse heights were recorded for several-thousand events in each run of this type. By moving the lead-glass array horizontally transverse to the beam, it was possible to obtain a series of runs in which each block was illuminated by  $e^+$  or  $e^-$  showers of several energies.

Reconstruction of the  $\pi^0$  from  $\Xi^0$  decays collected during normal data runs provided an alternate calibration technique. The two methods were consistent.

Not shown in Fig. 1 are helium bags located between MWPC's C1 to C5, a 1.5-meter-diameter Čerenkov counter between C5 and S2, and an additional MWPC 26 cm  $\times$  64 cm just upstream of S2. This MWPC improved the momentum measurement for the proton. Particle interactions in the frame of this MWPC and in the windows of the Čerenkov counter occasionally caused false vetos in S2. This effect was monitored with runs taken with and without S2 in the trigger. The analysis program included a small correction for this effect.

#### EVENT RECONSTRUCTION

The event reconstruction was done in several stages. First, the charged particles were fitted to the  $\Lambda$  hypothesis. The requirements were as follows:

- (1) The two charged tracks upstream of the spectrometer intersect in space in the decay volume.
- (2)  $X$  and  $Y$  views for each track correlate through C2 (wires oriented at  $45^\circ$  and  $135^\circ$  relative to the other chambers).
- (3) The track segments upstream and downstream of the spectrometer intersect in space approximately halfway through the magnet.
- (4) The bending angles determined from these trajectories yield momenta within broad, physically possible limits.
- (5) The decay hypothesis  $\Lambda \rightarrow p\pi^-$  is satisfied.

The mass spectrum for events which reached this final test is shown in Fig. 2(a).

Another step in the reconstruction involved searching for a pattern of energy deposition in the lead glass appropriate to two  $\gamma$  showers. Most of the triggers were caused by pion interactions in the glass with energy leaking into the blocks active in

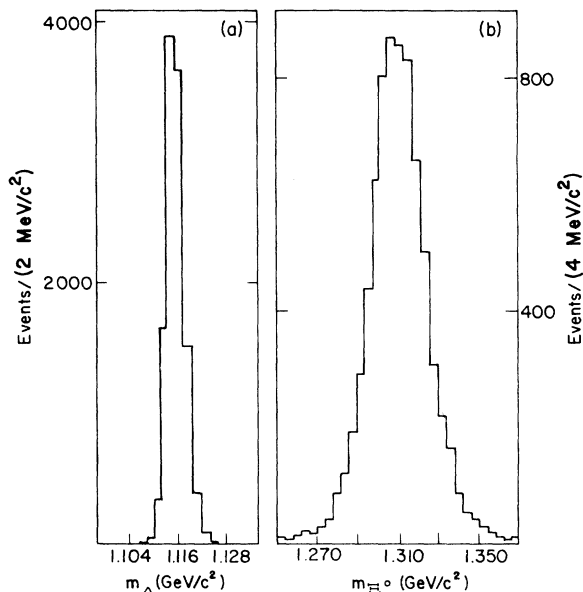


FIG. 2. (a) The proton- $\pi^-$  effective mass distribution for  $\Xi^0$  candidates with  $\nu e e$ 's identified as  $\Lambda$  hyperons. The distribution center is  $1.116 \text{ GeV}/c^2$  with a width of  $4.6 \text{ MeV}/c^2$  (FWHM). (b) The  $\Lambda$ - $\pi^0$  effective-mass distribution for a subset of  $\Xi^0$  candidates.

the trigger, and by accidental coincidences between a  $\Lambda$  and a neutral-particle conversion in the central block located in the neutral-beam path with energy leaking into neighboring blocks which were in the trigger. The  $\pi^-$ -induced background was reduced by requiring each observed  $\gamma$  to be at least 20 cm from the  $\pi^-$  at the glass. To eliminate neutral-beam background,  $\gamma$ 's with a majority of the energy in the central block were dropped from the  $\Xi^0$  analysis. An event was judged to contain a two- $\gamma$  pattern when two maxima in the energy deposition pattern were observed separated by at least two other blocks. About 1% of the raw triggers involved a satisfactory  $\Lambda$  and a two-shower pattern in the glass.

The step which reconstructed the  $\Xi^0$  employed a  $\chi^2$  fit. The input quantities were the  $\Lambda$ -momentum vector obtained from the proton and  $\pi^-$  tracks in the spectrometer and the energy and position of the two  $\gamma$ 's in the lead-glass calorimeter. Parameters included the three-momentum of the parent  $\Xi^0$ , the position of the  $\Xi^0$  decay vertex, and the decay angles at the  $\Xi^0 \rightarrow \Lambda\pi^0$  and  $\pi^0 \rightarrow \gamma\gamma$  decay vertex. Constraints required the two  $\gamma$ 's to fit the  $\pi^0$  mass, and the  $\Lambda$  and  $\pi^0$  to fit the  $\Xi^0$  mass. In addition, the reconstructed  $\Xi^0$  momentum vector was required to point to the production target. The errors used in the  $\chi^2$  for the energy and position of the  $\gamma$ 's were estimated. Because energy from the shower could be lost in the hole in the lead-

glass array as well as out the back of the array, the  $\chi^2$  does not follow a standard distribution for a 3-C fit. Figure 2b shows the  $\Lambda$ - $\pi^0$  effective mass for a sample of  $\Xi^0$  candidates in which the  $\Xi^0$  mass was left as a free parameter. The mass distribution was centered at 1.315 GeV/ $c^2$  with a width of 32 MeV/ $c^2$  [full width at half maximum (FWHM)].

#### DATA SELECTION

Two independent parameters were used to select a pure  $\Xi^0$  data sample. The  $\chi^2$  for the fit to the  $\Xi^0$  hypothesis has already been introduced. The second parameter was the radial distance ( $R^2$ ) from the center of the production target to the extrapolated position of the  $\Lambda$  at the target.  $R^2$  is particularly sensitive because the daughter  $\Lambda$  from  $\Xi^0$  decay rarely points near the production target, while  $\Lambda$  hyperons made in the target point there.  $\Lambda$ 's made in the target (beam  $\Lambda$ 's), in combination with accidental  $\gamma$ -like signals in the lead glass, will be shown to be the large part of the background. Thus, a cut accepting only events with a large  $R^2$  greatly reduces the background and eliminates a relatively small fraction of  $\Xi^0$  events.

Figure 3 shows a scatterplot of  $\Xi^0$  candidates. The two axes are  $R^2$  and  $\chi^2$ . The  $R^2$  projection shows the events in the regions  $\chi^2 < 20$  and  $\chi^2 > 20$ . The events with low  $\chi^2$  have generally large values of  $R^2$ , as expected for daughter  $\Lambda$ 's from  $\Xi^0$  decay. The events with high  $\chi^2$  have a sharp peak at  $R^2 = 0$ , indicating a background of target-produced  $\Lambda$ 's. In the scatterplot of the figure, it can be seen that these low- $R^2$  events have a flat  $\chi^2$  distribution for  $\chi^2 > 20$ . The  $\chi^2$  projection in the figure shows events with  $R^2 > 30$  mm<sup>2</sup>, a cut selecting  $\Xi^0$  decays. The  $\chi^2$  tail, which extends beyond the boundary shown in the figure, is greatly reduced by this  $R^2$  cut, while relatively few events are lost at low  $\chi^2$ .

Background in the event sample could arise from several sources. The background from beam  $\Lambda$ 's combined with accidental or  $\pi^-$ -induced lead-glass signals is evident in Fig. 3. This background was reproduced by analyzing "fake" events obtained by mixing  $\Lambda$  data from one event with lead-glass signals from other events with high  $\chi^2$ . The "fake" events with high  $\chi^2$  were normalized to the number of real events with high  $\chi^2$ . The normalized "fake" events remaining after  $\chi^2$  and  $R^2$  cuts then provided an estimate of this source of background. We estimate that the beam  $\Lambda$  background remaining in the final sample was  $2 \pm 1\%$ .

Another possible source of background would be beam  $\Lambda$  interactions with material in the neutral-beam line, producing a  $\pi^0$ . This source was minimized by requiring the reconstructed  $\Xi^0$  vertex

to be in the vacuum tank in the decay volume. Such interactions upstream of the veto counter S1 in Fig. 1 generally would not trigger the apparatus. Finally, the observed  $\Lambda$  vertex would be characteristic of a one-stage decay with the  $\Lambda$  lifetime. However, the  $\Lambda$ -vertex distribution was characteristic of a two-stage decay with relatively few events in the  $\Xi^0$  data sample with  $\Lambda$  vertices near S1. We estimate that this source is negligible.

A third class of possible background would be  $\Xi^0$  decay where only one  $\gamma$  is observed and one  $\gamma$ -like signal comes from an accidental or charged-particle-induced source. The detection efficiency for one- $\gamma$   $\Xi^0$  events is about five times the  $\Xi^0$  events where both  $\gamma$ 's hit the glass. The rate of single- $\gamma$  accidentals can be estimated from the rate of observation of an extra  $\gamma$  ("3 $\gamma$ " events) in the final event sample. This rate is 2%. In order to simulate the background, the extra  $\gamma$  in the 3 $\gamma$  sample was combined with 1 $\gamma$  Monte Carlo events to give a 1 $\gamma$  background sample. Of these, 20% fitted the  $\Xi^0$  selection criteria. It was determined by Monte Carlo that these events retain half the  $\Lambda$  polarization signal when analyzed as a 2 $\gamma$  event. Thus, the effect on the  $\alpha_{\Xi^0}$  measurement of this background is reduced. The effective unpolarized 1 $\gamma$  background is  $1 \pm 1\%$ .

The final data sample of 6075  $\Xi^0$  events was selected by requiring that  $\chi^2 < 20$  and that the daughter  $\Lambda$  not point to within 5.5 mm of the center of the beryllium target. We estimate  $3 \pm 2\%$  unpolarized background.

The  $\Xi^0$  hyperons in the final data sample have momenta between 80–300 GeV/ $c$ , with 181 GeV/ $c$  average momentum. The detection efficiency for the decay  $\Xi^0 \rightarrow \Lambda \pi^0$  was highly asymmetric in the  $\Xi^0$  rest frame: The requirement of observing two  $\gamma$ 's in the lead-glass preferentially selected high-momentum  $\pi^0$ 's, those emitted forward in the  $\Xi^0$  rest frame. Most  $\Lambda \rightarrow p \pi^-$  decays, however, were accepted.

#### POLARIZATION ANALYSIS

An unpolarized ensemble of  $\Xi^0$  hyperons at rest gives daughter  $\Lambda$ 's which are longitudinally polarized:

$$\vec{P}_\Lambda = \alpha_{\Xi^0} \hat{k}',$$

where  $\vec{P}_\Lambda$  is the polarization vector and  $\hat{k}'$  is a unit vector in the  $\Lambda$ -momentum direction. This can be understood rather easily because no reference direction in this system exists except the  $\Lambda$  momentum vector. It is useful to transform to a system in which the  $\Lambda$  is at rest. This is shown in Fig. 4. In this system, the  $\Lambda$  polarization must be along

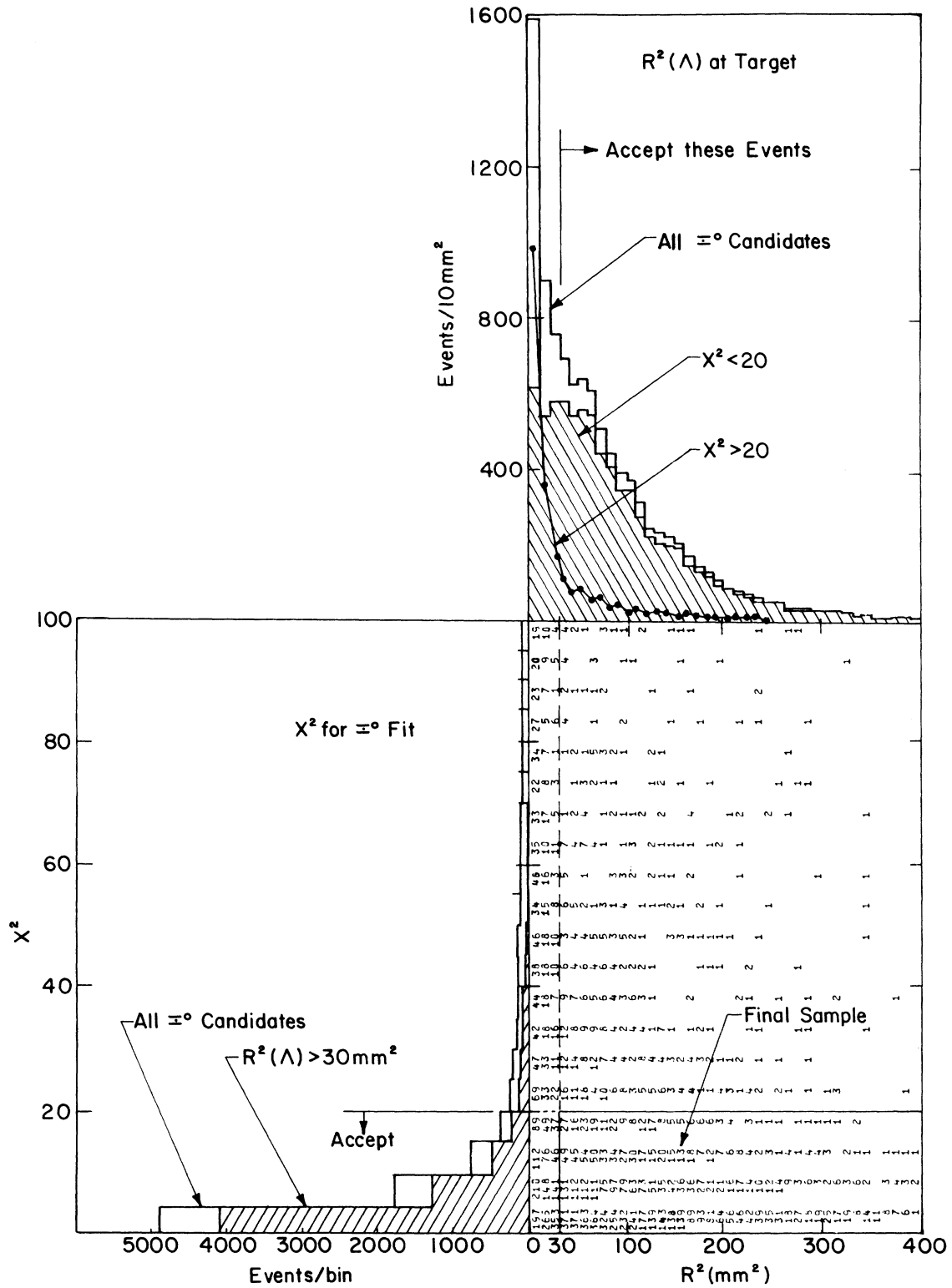


FIG. 3. A scatter plot of  $\Xi^0$  candidates. The two axes are the projection back to the production target of the  $\Lambda$ ,  $R^2$ , and  $\chi^2$  for the  $\Xi^0$  hypothesis. The final sample includes events with  $R^2 > 30$  mm<sup>2</sup> and  $\chi^2 < 20$ .

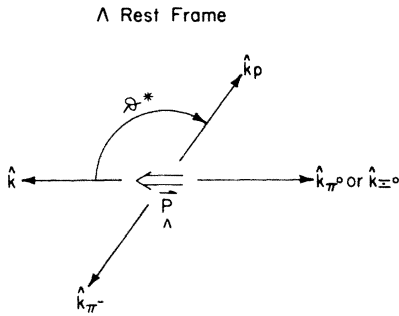


FIG. 4. The direction of the  $\Lambda$  polarization ( $\vec{P}_\Lambda$ ) from  $\Xi^0 \rightarrow \Lambda \pi^0$  decay is shown in the  $\Lambda$  rest frame, relative to the momentum directions of the  $\Xi^0$  and  $\Lambda^0 \rightarrow p \pi^-$  decays. Note that  $\cos \theta^* = \hat{k} \cdot \hat{k}_p$ .

$\hat{k}$  ( $-\hat{k}_{\Xi^0}$ ) and

$$\vec{P}_\Lambda = \alpha_{\Xi^0} \hat{k}.$$

This system is particularly convenient for discussing the self-analyzing property of  $\Lambda$  decay. The asymmetry is given by

$$\frac{dN}{d\Omega} = \frac{1}{4\pi} (1 + \alpha_\Lambda \vec{P}_\Lambda \cdot \hat{k}_p),$$

which can be written

$$\begin{aligned} \frac{dN}{d\Omega} &= \frac{1}{4\pi} (1 + \alpha_\Lambda \alpha_{\Xi^0} \hat{k} \cdot \hat{k}_p), \\ &= \frac{1}{4\pi} (1 + \alpha_\Lambda \alpha_{\Xi^0} \cos \theta^*), \end{aligned}$$

where the vectors are evident from the figure, and  $\alpha_\Lambda$  is the asymmetry parameter in  $\Lambda$  decay.

Thus, an analysis of the proton asymmetry in the  $\Lambda$  rest frame, relative to the  $\hat{k}$  ( $-\hat{k}_{\Xi^0}$ ) axis in this frame, gives  $\alpha_\Lambda \alpha_{\Xi^0}$ , with the relativistic spin transformations properly included.

The ingredients required to measure  $\alpha_{\Xi^0}$  are good center-of-mass resolutions for the  $\Xi^0$  and  $\Lambda$  decays, giving a precise value for  $\cos \theta^*$ , and well-understood detection efficiency. The angular resolution for  $\theta^*$  was determined by Monte Carlo calculation to be  $\sigma(\cos \theta^*) = 0.12$ . The average detection efficiency for  $\Lambda$ 's decaying within the decay zone was 85%. The uncorrected distribution of the proton in the  $\Lambda$  rest frame ( $\cos \theta^*$ ) in Fig. 5 shows the asymmetry imposed on the  $\Lambda$  decay by the polarization  $\alpha_{\Xi^0}$ . Part of the asymmetry, however, comes from the trigger requirement of a hit in S3, which preferentially selected high-momentum protons. This bias was removed by the analysis.

A  $\chi^2$  comparison between the  $\cos \theta^*$  distribution of the data (Fig. 5) and a simulated distribution was used to find  $\alpha_\Lambda \alpha_{\Xi^0}$ . The Monte Carlo simulation was based on the actual data. Monte Carlo events

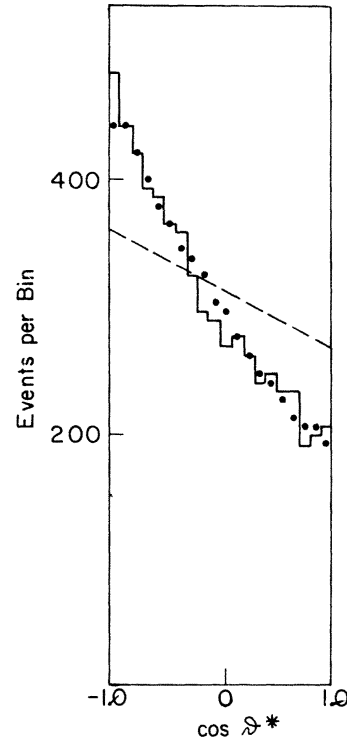


FIG. 5. The distribution of the proton from  $\Xi^0$  events projected onto the axis  $\hat{k}$  in the  $\Lambda$  rest frame. The dots are the Monte Carlo fit with  $\alpha_{\Xi^0} = -0.490$ . The dashed line represents the fit with  $\alpha_{\Xi^0} = 0$ , which indicates the detection efficiency of the apparatus.

were generated by replacing the values of  $\cos \theta_i^*$  for real events with a randomly generated  $\cos \theta_{MC}^*$ , all the other parameters of the real event being retained. The Monte Carlo event was then traced in the laboratory frame through the known experimental apertures. The process was repeated until 40 Monte Carlo events were accepted for each real event. Thus, the Monte Carlo events were assured of having the same momentum and vertex distributions as the real events. The simulated events tested only the acceptance in  $\cos \theta^*$ .

Now a Monte Carlo event thus generated must be weighted to correct for two effects. The sample of real events reflects a true asymmetry (the polarization  $\alpha_{\Xi^0}$ ). The Monte Carlo event generated from this sample will be biased if the acceptance in  $\cos \theta^*$  is not the same for each real event. The weight  $(1 + \alpha_\Lambda \alpha_{\Xi^0} \cos \theta_i^*)^{-1}$  for each Monte Carlo event removes the bias due to the polarized input distribution of the events  $\cos \theta_i^*$ . Thus weighted, the Monte Carlo events are unpolarized. The factor  $\alpha_{\Xi^0}$  in the weight is, of course, unknown.

The unpolarized Monte Carlo event is then weighted by  $(1 + \alpha_\Lambda \alpha_{\Xi^0} \cos \theta_{MC}^*)$ , obtaining a polarized distribution with the polarization  $\alpha_{\Xi^0}$ . Thus,

the weight for each Monte Carlo event was

$$W = \frac{1 + \alpha_{\Lambda} \alpha_{\Xi^0} \cos \theta_{MC}^*}{1 + \alpha_{\Lambda} \alpha_{\Xi^0} \cos \theta_i^*} \quad (1)$$

Different values of  $\alpha_{\Xi^0}$  may be tried until a minimum in  $\chi^2$  is found for the Monte Carlo fit to the  $\cos \theta^*$  distribution. In practice, the denominator of (1) was expanded according to  $(1+x)^{-1} = 1 - x + x^2$ , etc. This allowed the Monte Carlo distribution to be parameterized as a function of  $\alpha_{\Xi^0}$ , with sums such as

$$\sum_i \sum_{MC} \cos \theta_{MC}^* \cos \theta_i^*$$

being accumulated as the Monte Carlo was generated, for simulated events in each of 20  $\cos \theta^*$  bins. The  $\chi^2$  of the Monte Carlo fit to the data was then written as a function of  $\alpha_{\Xi^0}$ , and the minimum was determined by Newton's method. An increase of  $\chi^2$  by one from its minimum determined the quoted error for  $\alpha_{\Xi^0}$ .

The Monte Carlo fit to the  $\cos \theta^*$  distribution is shown by the dots in Fig. 5. A  $\chi^2$  of 16 for 19 degrees of freedom was obtained for the fit. For  $\alpha_{\Xi^0} = 0$ , on the other hand, the  $\chi^2$  was 210 and is also shown in the figure.

Several tests were made on the analysis. Runs were taken without the lead-glass trigger to select a sample of beam  $\Lambda$ 's. The polarization for beam  $\Lambda$ 's was measured to be zero. The fake events with low  $\chi^2$  for  $\Xi^0$  decay were found to have  $\alpha_{\Xi^0} = 0$ . This tested for bias due to any correlation between the  $\chi^2$  obtained from the  $\Xi^0$  fit and the decay proton direction.

It should be emphasized that apparatus biases correlate weakly with the daughter- $\Lambda$  polarization direction. The daughter  $\Lambda$ 's from  $\Xi^0$  decay are polarized in the  $\Xi^0$  rest frame so that in the laboratory frame the net  $\Lambda^0$  polarization in any direction is small.

## RESULT

An analysis of 6075  $\Xi^0$  decays gave  $\alpha_{\Lambda} \alpha_{\Xi^0} = -0.317 \pm 0.027$  after adjustment by the factor 1.03 for  $(3 \pm 2)\%$  background. With  $\alpha_{\Lambda} = 0.647$ ,<sup>5</sup>  $\alpha_{\Xi^0} = -0.490 \pm 0.042$ .<sup>6</sup> Table I compares our result with previous measurements. The average of the previous measurements is  $-0.453 \pm 0.061$ .

Our value of  $\alpha_{\Xi^0}$  along with a recent high-statis-

TABLE I. Measurements of the  $\Xi^0$  asymmetry parameter.

| No. of Events | $\alpha_{\Xi^0}$   | Reference       |
|---------------|--------------------|-----------------|
| 146           | $-0.13 \pm 0.17$   | 7               |
| 739           | $-0.43 \pm 0.09$   | 8               |
| 130           | $-0.84 \pm 0.27$   | 9               |
| 652           | $-0.54 \pm 0.10$   | 10              |
| 6075          | $-0.490 \pm 0.042$ | This experiment |

tics determination of the  $\Xi^0$  lifetime<sup>11</sup> allow a considerably improved test of the  $\Delta I = \frac{1}{2}$  rule in  $\Xi$  decay. The  $\Delta I = \frac{1}{2}$  rule predicts  $\alpha^0/\alpha^- = 1$  and  $\tau^0/\tau^- = 2$ , where the superscript refers to the sign of the  $\Xi$ . Including phase space, these ratios become  $\alpha^0/\alpha^- = 0.975$  and  $\tau^0/\tau^- = 2.067$ . Other radiative corrections are smaller<sup>4</sup> but in the same direction. The world averages are  $\alpha_{\Xi^-} = -0.392 \pm 0.021$ ,<sup>7,8,10,12,13</sup>  $\tau_{\Xi^-} = (1.652 \pm 0.023) \times 10^{-10}$  sec,<sup>8,10,13</sup> and  $\tau_{\Xi^0} = (2.89 \pm 0.10) \times 10^{-10}$  sec.<sup>11</sup> Comparison of asymmetry parameters and lifetimes each indicate violation of the  $\Delta I = \frac{1}{2}$  rule. The decay is primarily  $s$  wave<sup>14</sup> so the disagreement in the lifetime prediction effectively sets the  $s$ -wave violation, leaving the  $p$ -wave violation mainly determined by the disagreement in asymmetry parameters. From the formulation of Ref. 3, there is  $4.1 \pm 1.5\%$  violation in the  $s$ -wave amplitudes and a  $22 \pm 9\%$  violation in the  $p$  wave, with no phase-space corrections. With phase-space corrections, the violations are  $5.0 \pm 1.5\%$  for the  $s$ -wave and  $25 \pm 9\%$  for the  $p$ -wave amplitudes.

This result represents a considerable improvement in accuracy over the results available when Ref. 1 was published. The presence of  $\Delta I = \frac{3}{2}$  amplitudes is fairly clear. The violation of the  $\Delta I = \frac{1}{2}$  rule appears to be quite large for the  $p$ -wave amplitude of  $\Xi$  decay, although this latter conclusion would benefit from further improvements in statistical accuracy.

## ACKNOWLEDGMENTS

We thank the staff at Fermilab for their help, in particular C. Brown and H. Haggerty. E. Behr, S. Fraser, and G. Ott provided technical support. This work was supported in part by the U. S. Department of Energy and in part by the National Science Foundation.

\*Present address: Brookhaven National Laboratory, Upton, N.Y. 11973.

†Present address: Lawrence Berkeley Laboratory, Berkeley, Cal. 94720.

‡Present address: Physics Department, Rutgers—The State University, Piscataway, N.J. 08854.

§Present address: Ford Motor Company, Allen Park, Michigan 48101.

- †Present address: Bell Laboratories, Holmdel, N. J. 07733.
- <sup>1</sup>O. E. Overseth, *Rev. Mod. Phys.* 48, S242 (1976).
- <sup>2</sup>A. A. Belavin and L. M. Narodetsky, *Phys. Lett.* 26B, 668 (1968).
- <sup>3</sup>O. E. Overseth and S. Pakvasa, *Phys. Rev.* 184, 1663 (1969).
- <sup>4</sup>G. W. Intemann, *Phys. Rev. D* 10, 3753 (1974).
- <sup>5</sup>O. E. Overseth and R. F. Roth, *Phys. Rev. Lett.* 19, 391 (1967); W. Cleland *et al.*, *Nucl. Phys.* B40, 221 (1972).
- <sup>6</sup>A preliminary number for  $\alpha_{\pm 0}$  ( $= -0.566 \pm 0.062$ ) from a subset of these data was quoted by G. Bunce *et al.*, in *High Energy Physics with Polarized Beams and Targets*, proceedings of the Argonne Symposium, 1976, edited by M. L. Marshak (AIP, New York, 1976), p. 280.
- <sup>7</sup>J. P. Berge *et al.*, *Phys. Rev.* 147, 945 (1966).
- <sup>8</sup>P. M. Dauber *et al.*, *Phys. Rev.* 179, 1262 (1969).
- <sup>9</sup>C. Mayeur *et al.*, *Nucl. Phys.* B47, 333 (1972).
- <sup>10</sup>C. Baltay *et al.*, *Phys. Rev. D* 9, 49 (1974).
- <sup>11</sup>G. Zech *et al.*, *Nucl. Phys.* B124, 413 (1977).
- <sup>12</sup>G. M. D. Bingham *et al.*, *Phys. Rev. D* 1, 3010 (1970).
- <sup>13</sup>R. L. Cool *et al.*, *Phys. Rev. D* 10, 792 (1974). The average is from the Particle Data Group, *Rev. Mod. Phys.* 48, S1 (1976).
- <sup>14</sup>This is deduced from measurements of  $\Phi_{\pm 0}$  (Refs. 7, 8, 10). A value of  $\Phi$  near 0 indicates *s*-wave dominance; predominantly *p*-wave decay would give  $\Phi$  near 180°. The world average is  $\Phi_{\pm 0} = 20.7^\circ \pm 11.7^\circ$ , from the Particle Data Group (Ref. 13).



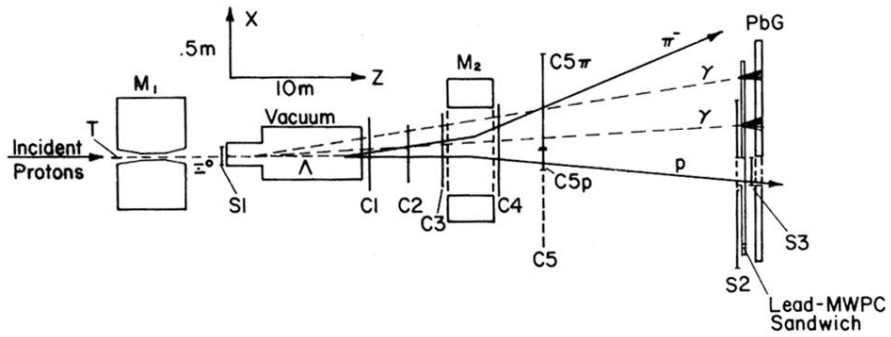


FIG. 1. A typical  $\Xi^0 \rightarrow \Lambda \pi^0$ ,  $\Lambda \rightarrow p \pi^-$ ,  $\pi^0 \rightarrow \gamma \gamma$  event is superimposed on the top view of the apparatus. S1–S3 are scintillation counters; V is the decay volume; C1–C5 are MWPC's; M2 is the analyzing magnet; PbG is the lead-glass array. C5p and C5 $\pi$  represent two sections of C5 used in the  $\Xi^0$  trigger. The trigger consisted of  $T(\Xi^0) = C1 \cdot C2 \cdot C3 \cdot C4 \cdot C5p \cdot C5\pi \cdot S3 \cdot G \cdot S1 \cdot S2$ , where G represents a sum of lead-glass signals (see text).

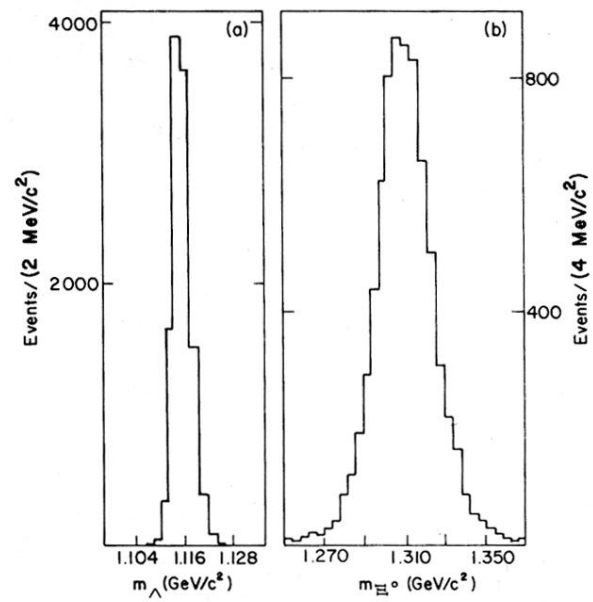


FIG. 2. (a) The proton- $\pi^-$  effective mass distribution for  $\Xi^0$  candidates with vee's identified as  $\Lambda$  hyperons. The distribution center is  $1.116 \text{ GeV}/c^2$  with a width of  $4.6 \text{ MeV}/c^2$  (FWHM). (b) The  $\Lambda$ - $\pi^0$  effective-mass distribution for a subset of  $\Xi^0$  candidates.

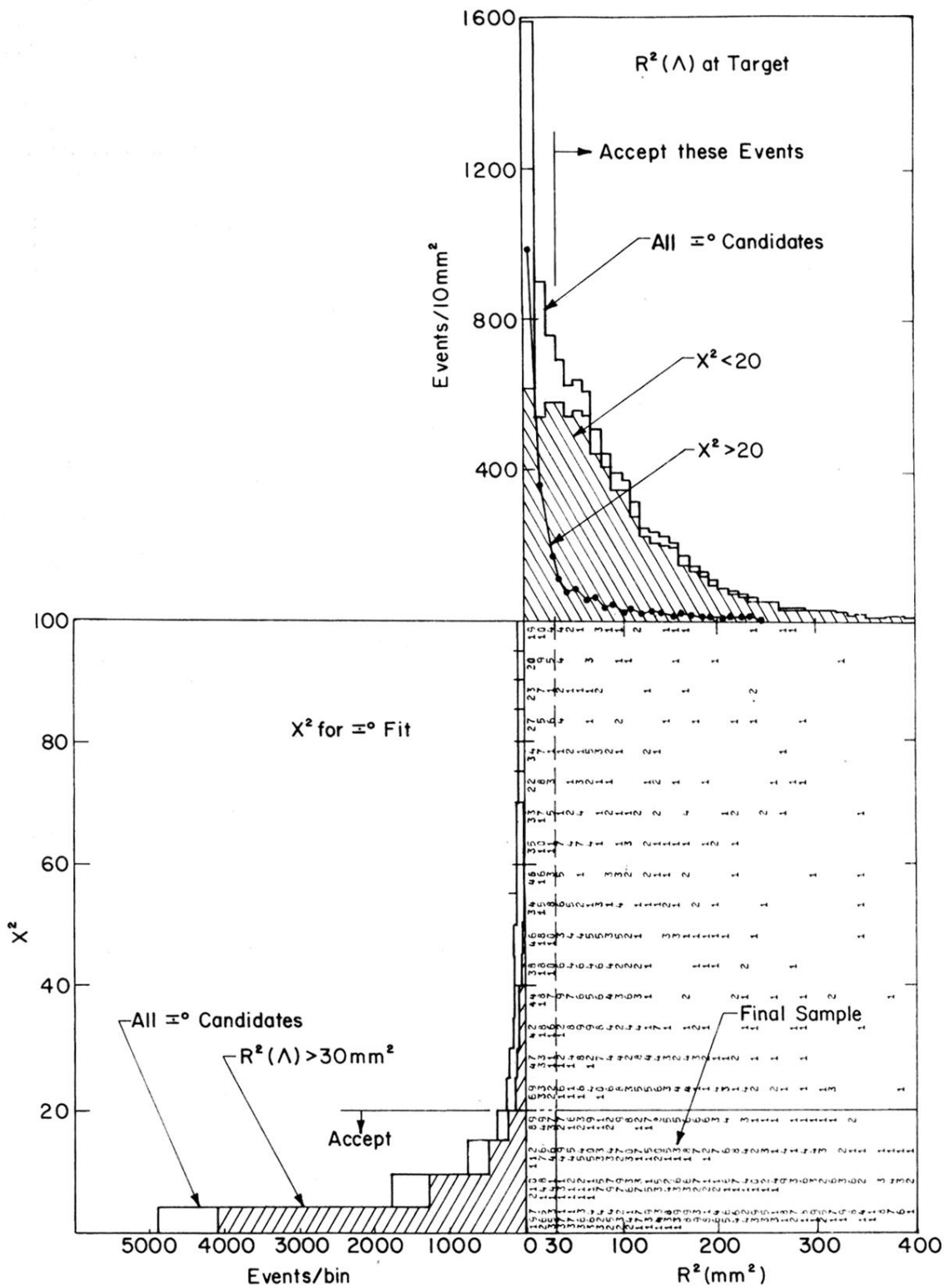


FIG. 3. A scatter plot of  $\Xi^0$  candidates. The two axes are the projection back to the production target of the  $\Lambda$ ,  $R^2$ , and  $\chi^2$  for the  $\Xi^0$  hypothesis. The final sample includes events with  $R^2 > 30 \text{mm}^2$  and  $\chi^2 < 20$ .

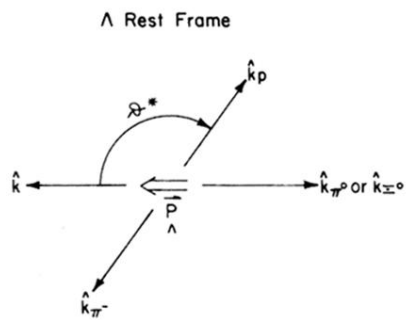


FIG. 4. The direction of the  $\Lambda$  polarization ( $\hat{P}_\Lambda$ ) from  $\Xi^0 \rightarrow \Lambda \pi^0$  decay is shown in the  $\Lambda$  rest frame, relative to the momentum directions of the  $\Xi^0$  and  $\Lambda^0 \rightarrow p \pi^-$  decays. Note that  $\cos \theta^* = \hat{h} \cdot \hat{k}_p$ .

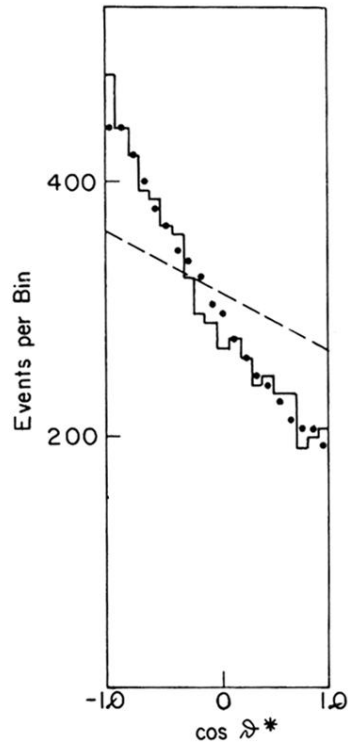


FIG. 5. The distribution of the proton from  $\Xi^0$  events projected onto the axis  $\hat{k}$  in the  $\Lambda$  rest frame. The dots are the Monte Carlo fit with  $\alpha_{\Xi^0} = -0.490$ . The dashed line represents the fit with  $\alpha_{\Xi^0} = 0$ , which indicates the detection efficiency of the apparatus.